

‘Lissajous-like’ trajectories in optical tweezers

R. F. Hay,¹ G. M. Gibson,¹ S. H. Simpson,² M. J. Padgett,¹ and
D. B. Phillips^{1,*}

¹ School of Physics and Astronomy, Glasgow University, Glasgow, G12 8QQ, Scotland, UK

² ASCR, Institute of Scientific Instruments, Královopolská 147, 612 64 Brno, Czech Republic

*david.phillips@glasgow.ac.uk

Abstract: When a microscopic particle moves through a low Reynolds number fluid, it creates a flow-field which exerts hydrodynamic forces on surrounding particles. In this work we study the ‘Lissajous-like’ trajectories of an optically trapped ‘probe’ microsphere as it is subjected to time-varying oscillatory hydrodynamic flow-fields created by a nearby moving particle (the ‘actuator’). We show a breaking of time-reversal symmetry in the motion of the probe when the driving motion of the actuator is itself time-reversal symmetric. This symmetry breaking results in a fluid-pumping effect, which arises due to the action of both a time-dependent hydrodynamic flow and a position-dependent optical restoring force, which together determine the trajectory of the probe particle. We study this situation experimentally, and show that the form of the trajectories observed is in good agreement with Stokesian dynamics simulations. Our results are related to the techniques of active micro-rheology and flow measurement, and also highlight how the mere presence of an optical trap can perturb the environment it is in place to measure.

© 2015 Optical Society of America

OCIS codes: (140.7010) Laser trapping; (170.4520) Optical confinement and manipulation; (350.4855) Optical tweezers or optical manipulation.

References and links

1. J. Happel and H. Brenner, *Low Reynolds Number Hydrodynamics: with Special Applications to Particulate Media* (Springer Science & Business Media, 2012) vol. 1.
2. E. M. Purcell, “Life at low reynolds number,” *Am. J. Phys.* **45**, 3–11 (1977).
3. A. Shapere and F. Wilczek, “Geometry of self-propulsion at low reynolds number,” *J. Fluid Mech.* **198**, 557–585 (1989).
4. J. Elgeti, R. G. Winkler, and G. Gompper, “Physics of microswimmers: single particle motion and collective behavior: a review,” *Rep. Prog. Phys.* **78**, 056601 (2015).
5. J.-C. Meiners and S. R. Quake, “Direct measurement of hydrodynamic cross correlations between two particles in an external potential,” *Phys. Rev. Lett.* **82**, 2211 (1999).
6. T. Niedermayer, B. Eckhardt, and P. Lenz, “Synchronization, phase locking, and metachronal wave formation in ciliary chains,” *Chaos* **18**, 037128 (2008).
7. J. Kotar, M. Leoni, B. Bassetti, M. C. Lagomarsino, and P. Cicuta, “Hydrodynamic synchronization of colloidal oscillators,” *Proc. Natl. Acad. Sci. U.S.A.* **107**, 7669–7673 (2010).
8. A. Curran, M. P. Lee, M. J. Padgett, J. M. Cooper, and R. Di Leonardo, “Partial synchronization of stochastic oscillators through hydrodynamic coupling,” *Phys. Rev. Lett.* **108**, 240601 (2012).
9. J. Kotar, L. Debono, N. Bruot, S. Box, D. Phillips, S. Simpson, S. Hanna, and P. Cicuta, “Optimal hydrodynamic synchronization of colloidal rotors,” *Phys. Rev. Lett.* **111**, 228103 (2013).
10. D. R. Brumley, M. Polin, T. J. Pedley, and R. E. Goldstein, “Metachronal waves in the flagellar beating of *volvox* and their hydrodynamic origin,” arXiv preprint arXiv:1505.02423 (2015).

11. A. Najafi and R. Golestanian, "Simple swimmer at low reynolds number: Three linked spheres," *Phys. Rev. E* **69**, 062901 (2004).
12. S. Maruo, H. Inoue, "Optically driven micropump produced by three-dimensional two-photon microfabrication," *Am. Inst. Phys.* (2006).
13. J. Leach, H. Mushfique, R. di Leonardo, M. Padgett, and J. Cooper, "An optically driven pump for microfluidics," *Lab Chip* **6**, 735–739 (2006).
14. D. Phillips, M. Padgett, S. Hanna, Y.-L. Ho, D. Carberry, M. Miles, and S. Simpson, "Shape-induced force fields in optical trapping," *Nat. Photon.* **8**, 400–405 (2014).
15. A. Ashkin, J. Dziedzic, J. Bjorkholm, and S. Chu, "Observation of a single-beam gradient force optical trap for dielectric particles," *Opt. Lett.* **11**, 288–290 (1986).
16. A. Ashkin, "Forces of a single-beam gradient laser trap on a dielectric sphere in the ray optics regime," *Biophys. J.* **61**, 569 (1992).
17. S. C. Kuo and M. P. Sheetz, "Force of single kinesin molecules measured with optical tweezers," *Science* **260**, 232–234 (1993).
18. Y. Sokolov, D. Frydel, D. G. Grier, H. Diamant, and Y. Roichman, "Hydrodynamic pair attractions between driven colloidal particles," *Phys. Rev. Lett.* **107**, 158302 (2011).
19. R. Di Leonardo, J. Leach, H. Mushfique, J. Cooper, G. Ruocco, and M. Padgett, "Multipoint holographic optical velocimetry in microfluidic systems," *Phys. Rev. Lett.* **96**, 134502 (2006).
20. S. R. Kirchner, S. Nedev, S. Carretero-Palacios, A. Mader, M. Opitz, T. Lohmüller, and J. Feldmann, "Direct optical monitoring of flow generated by bacterial flagellar rotation," *Appl. Phys. Lett.* **104**, 093701 (2014).
21. S. Nedev, S. Carretero-Palacios, S. Kirchner, F. Jäckel, and J. Feldmann, "Microscale mapping of oscillatory flows," *Appl. Phys. Lett.* **105**, 161113 (2014).
22. L. Hough and H. Ou-Yang, "Correlated motions of two hydrodynamically coupled particles confined in separate quadratic potential wells," *Phys. Rev. E* **65**, 021906 (2002).
23. C. D. Mellor, M. A. Sharp, C. D. Bain, and A. D. Ward, "Probing interactions between colloidal particles with oscillating optical tweezers," *J. Appl. Phys.* **97**, 103114 (2005).
24. M. Atakhorrami, D. Mizuno, G. Koenderink, T. Liverpool, F. MacKintosh, and C. Schmidt, "Short-time inertial response of viscoelastic fluids measured with brownian motion and with active probes," *Phys. Rev. E* **77**, 061508 (2008).
25. D. L. Ermak and J. McCammon, "Brownian dynamics with hydrodynamic interactions," *J. Chem. Phys.* **69**, 1352–1360 (1978).
26. J. Rotne and S. Prager, "Variational treatment of hydrodynamic interaction in polymers," *J. Chem. Phys.* **50**, 4831–4837 (1969).
27. D. B. Phillips, L. Debono, S. H. Simpson, and M. J. Padgett, "Optically controlled hydrodynamic micro-manipulation," *Proc. SPIE* **9548**, 95481A (2015).
28. H. Nagar and Y. Roichman, "Collective excitations of hydrodynamically coupled driven colloidal particles," *Phys. Rev. E* **90**, 042302 (2014).
29. S. Box, L. Debono, D. Phillips, and S. Simpson, "Transitional behavior in hydrodynamically coupled oscillators," *Phys. Rev. E* **91**, 022916 (2015).
30. B. A. Nemet and M. Cronin-Golomb, "Microscopic flow measurements with optically trapped microprobes," *Opt. Lett.* **27**, 1357–1359 (2002).
31. A. Béruit, A. Petrosyan, and S. Ciliberto, "Energy flow between two hydrodynamically coupled particles kept at different effective temperatures," *Europhys. Lett.* **107**, 60004 (2014).
32. Y. Roichman, B. Sun, A. Stolarski, and D. G. Grier, "Influence of nonconservative optical forces on the dynamics of optically trapped colloidal spheres: the fountain of probability," *Phys. Rev. Lett.* **101**, 128301 (2008).
33. J. E. Curtis, B. A. Koss, and D. G. Grier, "Dynamic holographic optical tweezers," *Opt. Commun.* **207**, 169–175 (2002).
34. G. M. Gibson, J. Leach, S. Keen, A. J. Wright, and M. J. Padgett, "Measuring the accuracy of particle position and force in optical tweezers using high-speed video microscopy," *Opt. Express* **16**, 14561–14570 (2008).
35. J. Liesener, M. Reicherter, T. Haist, and H. Tiziani, "Multi-functional optical tweezers using computer-generated holograms," *Opt. Commun.* **185**, 77–82 (2000).
36. R. W. Bowman, G. M. Gibson, A. Linnenberger, D. B. Phillips, J. A. Grieve, D. M. Carberry, S. Serati, M. J. Miles, and M. J. Padgett, "'Red tweezers': Fast, customisable hologram generation for optical tweezers," *Comput. Phys. Commun.* **185**, 268–273 (2014).

1. Introduction

Hydrodynamic interactions in low Reynolds number environments, where the viscous drag dominates over inertial forces, frequently produce counter-intuitive effects. The suppression of inertia causes objects to come to rest nearly instantaneously upon the cessation of the forces propelling them [1]. Motile microscopic organisms experience water at low Reynolds num-

ber, and have evolved specialised swimming strategies to propel themselves through such an environment [2]. As micro-swimmers cannot rely on the inertia of the surrounding fluid to achieve propulsion, they must perform periodic deformations that break time-reversal symmetry, achieved for example, by using corkscrewing motions or the beating of flexible flagella [3, 4]. The ‘Scallop theorem’ states that the breaking of time-reversal symmetry is a requirement in the generation of a non-zero cycle-averaged flow-field in the low Reynolds number limit, which can be harnessed to achieve forward motion or pump fluid.

The flow-field generated around a moving micro-particle exerts hydrodynamic forces on surrounding particles, acting to weakly couple together the motion of neighbouring objects [5]. This coupling can lead to the synchronisation of systems even when the only interaction forces are hydrodynamic [6–8]. Synchronisation is often observed in biological systems, such as the beating of cilia, where the importance of hydrodynamic interactions is still an open question [9, 10]. More generally, an understanding of the physics at work in low Reynolds number environments has helped our understanding of the connection between the form and the function of micro-scale biological systems. This understanding may also facilitate the development of artificial micro-swimmers and fluid pumps, and inform the growing field of micro-robotics [11–14].

Many low Reynolds number micro-particle systems have been understood with the aid of optical tweezers, which are formed by tightly focused beams of light [15]. Optical tweezers can be used to manipulate, and exert well-defined forces on, microscopic particles [16, 17] and enable the direct measurement of hydrodynamic interactions between these particles [18]. In this paper we study a simple system of two hydrodynamically interacting optically trapped particles. The first trapped microsphere (here referred to as the ‘actuator’) is periodically driven around a closed trajectory. We then observe the response of the second microsphere (the ‘probe’) as it is subjected to the time-varying oscillatory flow-field created by the movement of the actuator. The probe undergoes a variety of closed-loop trajectories that bear a similarity to Lissajous

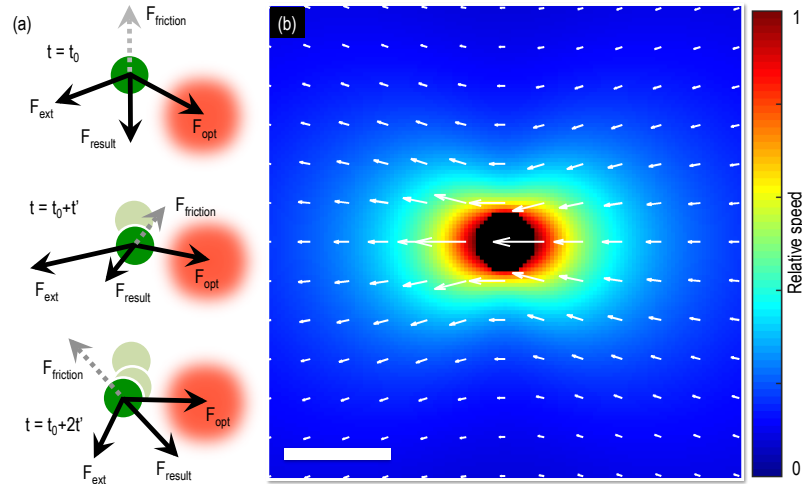


Fig. 1. (a) Schematic showing how the trajectory of a microsphere is calculated at each simulation time-step from the balance of external forces, F_{ext} (such as hydrodynamic and stochastic thermal forces), optical forces, F_{opt} , and frictional forces, $F_{friction}$. (b) A map of the flow-field (relative to the velocity of the microsphere) around an isolated microsphere of $5 \mu\text{m}$ in diameter, as it is translated left. Arrows indicate the amplitude and direction of the flow. The white scale bar represents $10 \mu\text{m}$.

curves, the exact form of which depend upon the motion of the actuator. In particular we contrast two different experimental configurations: firstly when the actuator is driven around a non time-reversal symmetric trajectory, and secondly, when the actuator's trajectory is time-reversal symmetric. We show that the introduction of a stationary optical trap constraining the motion of the probe microsphere causes a breaking of time-reversal symmetry of the system, even when the oscillating driving force is itself time-reversal symmetric. This symmetry breaking induces a small, non-zero cycle-averaged flow-field, and results in a fluid pumping action in a direction orthogonal to that of the driving force. We first describe numerical simulations, followed by experimental validation. Our work has applications to flow sensing [19–21], and is also related to the techniques of active micro-rheology [22–24], and highlights a mechanism by which stationary ‘passive’ optical traps can perturb the environment that they are in place to measure.

2. Stokesian dynamics simulations

2.1. Simulation method

We first simulate the evolution of the two bead actuator and probe system using a Stokesian dynamics protocol to numerically integrate a discretised Langevin equation [1, 25]. Equation (1) describes the velocity of each degree of freedom of each microsphere in a system of N microspheres, from the balance of forces over a series of small time-steps (see Fig. 1(a)):

$$m_i \frac{d^2 x_i}{dt^2} = - \sum_{j=1}^{3N} (\xi_{ij} \frac{dx_j}{dt}) + \kappa_j (\delta x_j) + \sum_{j=1}^{3N} \alpha_{ij} f_j, \quad (1)$$

where i and j index the degrees of freedom of all particles, i.e. $1 \leq i, j \leq 3N$, indexing three translational degrees of freedom for each of N particles. m_i is the mass of the particle (which is of course the same for each degree of freedom indexed on a particular particle), x_i denotes the coordinate of a particular degree of freedom of a particular particle, and t is time. ξ is the $3N \times 3N$ element friction tensor describing the friction of the whole system of particles (each element indexed by i and j), κ_j is the stiffness of each optical trap in a particular degree of freedom, δx_j is the displacement of particle j from the centre of its associated optical trap, f is a stochastic force due to Brownian motion, and α is a tensor describing the coupling of Brownian fluctuations on nearby particles, which can be calculated from ξ . As we are working in the low Reynolds number limit, we set the left hand side to zero: the particles are always considered to be moving at a constant velocity within each time-step. More detail of Eq. (1) can be found in [25].

The first term on the right hand side (RHS) describes the hydrodynamic drag forces on each particle, encapsulating the interactions with neighbouring particles through disturbances in the fluid. The second term on the RHS describes the optical forces on each particle, assuming that the displacements are small and so optical force is linearly proportional to the particle's distance from the centre of the optical trap. The third term on the RHS describes the thermal forces acting on each particle. In this work we are mainly interested in time-averaged characteristics of the system and so ‘turn off’ Brownian motion by setting this term to zero. We use the Rotne Prager approximation to calculate the friction tensor ξ [26]. As ξ depends on the configuration of the particles, this is recalculated at each time-step for every new configuration. An estimate of the surrounding flow-field can also be mapped out by calculating the hydrodynamic forces felt by an additional small free-floating bead at a grid of positions. Fig. 1(b) shows the characteristic flow-field around a single translating microsphere passing through its centre and in the plane of its motion.

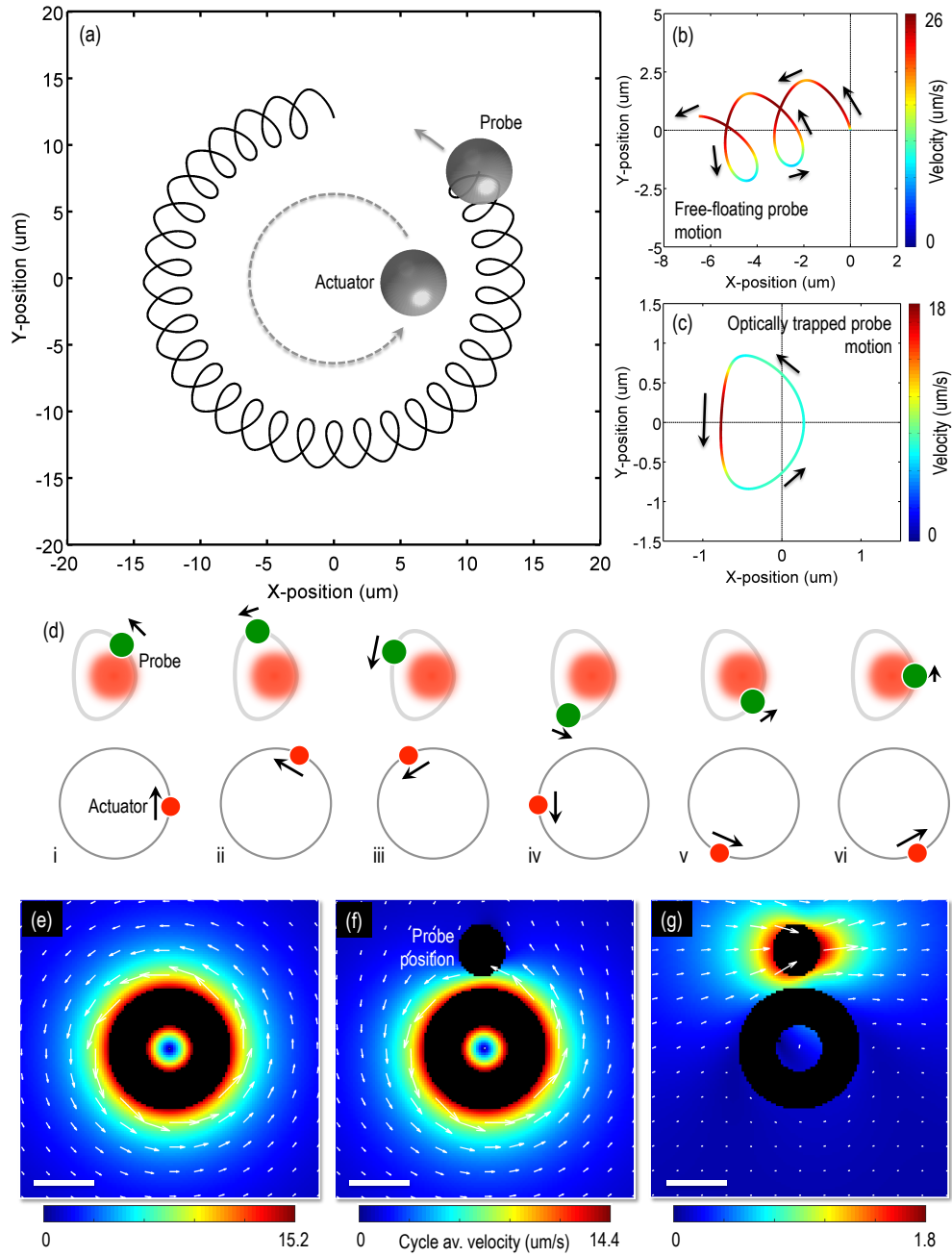


Fig. 2. Simulations of the system with a non time-reversal symmetric actuator trajectory. (a) Trajectory of a free-floating probe microsphere as it is driven by the rotary motion of the actuator in the absence of thermal forces. (b) Velocity of the free-floating probe along its trajectory. (c) Trajectory and velocity of the probe when it is constrained by an optical trap. (d) Schematic of the relative positions of the actuator and probe microspheres during one actuator cycle. The relative size of the probe trajectory has been exaggerated compared to both the probe's size, and the actuator trajectory, for clarity. (e) Cycle averaged flow-field around an isolated actuator. (f) Cycle averaged flow-field around the actuator while the probe is held in a stationary optical trap. (g) Difference in the flow-field between (e) and (f). In each case the white scale bars represent $10\mu\text{m}$.

We note that there are a number of caveats to be aware of when using the Stokesian dynamics simulation described here. Our simulations ignore rotations of the microspheres about their own centres, and the forces on each particle are calculated at the centre of each sphere. The Rotne Praga approximation assumes that the particles are at least several diameters from one another. The time-step for the numerical integration must also be chosen appropriately. Here we use a time step of 0.1 ms, chosen as this is much smaller than the relaxation time of the optically trapped particles, and much larger than the correlation time of thermal motion (should we include it). These assumptions are all reasonable for the situations we consider here. In addition, our simulation method has been previously shown to correctly account for hydrodynamic interactions in a variety of many particle systems, and is widely used in the literature [27–29].

2.2. *Non time-reversal symmetric actuator trajectory*

We first study the evolution of the system when an actuator microsphere of $5\ \mu\text{m}$ in diameter, is driven anticlockwise in a circular trajectory with a radius of $6\ \mu\text{m}$, at a rate of 2 Hz, corresponding to a constant speed of $75.4\ \mu\text{m/s}$, as shown in Fig. 2. The actuator's trajectory is not symmetric upon time-reversal, and therefore the cycle-averaged flow-field it creates is non-zero. This results in a net force on the probe per cycle acting to push it in an anticlockwise direction around the centre of motion of the actuator. Figures 2(a) and 2(b) show the simulated trajectory of a free-floating (i.e. its position is not constrained by an optical trap) probe microsphere of $5\ \mu\text{m}$ in diameter, in the absence of Brownian motion. As shown in Fig. 2(a), when the probe is initially placed at $x = 0\ \mu\text{m}$, $y = 12\ \mu\text{m}$, it undergoes a spiralling motion as it is pushed around the actuator, with each spiral corresponding to one full rotation of the actuator. This spiralling motion arises due to the changing distance and angle (relative to the instantaneous direction of motion of the actuator) between the two microspheres. The radial displacements of the probe exactly cancel over one cycle of the actuator. The azimuthal displacements of the probe within one actuator cycle, though smaller than the radial displacements (as can be understood by the flow-field around a moving bead shown in Fig 1(b)), do not cancel, as the actuator is further from the probe on the returning portion of its cycle. The relative magnitude of the force on the probe throughout different parts of its trajectory are reflected in the speed that it moves, as shown in Fig. 2(b). Figures 2(a) and 2(b) also point towards methods to indirectly *hydrodynamically* manipulate free-floating objects using flows generated by nearby optically trapped particles [27].

The introduction of a stationary optical trap constraining the motion of the probe causes the probe's spiral trajectory to transform into a closed asymmetric orbit around the position of the optical trap. The probe's trajectory is now defined by the changing balance between hydrodynamic, optical, and frictional forces. Figure 2(c) shows the velocity of the probe as it orbits the trap. The cycle-averaged position of the probe encodes the cycle-averaged hydrodynamic force exerted on it by the actuator. Therefore, constraining the motion of the probe using a stationary optical trap enables the measurement of the cycle-averaged flow-field, even in the presence of thermal forces (which can be averaged out over many cycles) [30]. However, although the probe enables an accurate estimate of the flow rate at a *single-point* (averaged over the surface of the probe bead), this measurement will itself perturb the flow-field of the entire system. For example, Figs. 2(e) and 2(f) show the cycle averaged flow-field around the actuator, without (Fig. 2(e)), and with (Fig. 2(f)), the motion of the probe constrained by a stationary optical trap. Figure 2(g) shows the difference in the cycle-averaged flow-field between Fig. 2(e) and Fig. 2(f). The cycle-averaged flow-field of the whole system is modified due to the presence of the stationary optical trap, and therefore care must be taken if performing a *multi-point* flow velocity measurement using several optically trapped probe particles. For example, in Eq. (1), coupling between particles enters through the friction tensor ξ , and depends upon the magni-

tude of external forces (e.g. optical or stochastic, the last two terms on the RHS of Eq. (1)) that particles are subjected to. Therefore coupling between several optically trapped flow probes will effect a multi-point velocity measurement, as discussed in [19]. We now investigate how the presence of an optical trap constraining the motion of the probe microsphere modifies the flow-field for a time-reversible system, with a zero cycle-average.

2.3. Time-reversal symmetric actuator trajectory

The actuator is now driven in only one dimension, sinusoidally and parallel to the x-axis at a rate of 2 Hz, with an amplitude of $6\text{ }\mu\text{m}$, corresponding to a *maximum* speed of $75.4\text{ }\mu\text{m/s}$. As this motion is symmetric upon time-reversal, the cycle-averaged flow generated around it is zero (in the absence of Brownian motion). Figure 3(a) shows the simulated trajectory of the free-floating probe microsphere experiencing the time-reversal symmetric flow-field, again in the absence of Brownian motion. As expected, analogously to the actuator, the probe also periodically retraces the same path over each cycle. The displacement of the probe in the y-direction is due to the y-component of the flow-field generated around a translating bead which can be seen in Fig. 1(b).

We now introduce a stationary optical trap constraining the motion of the probe microsphere.

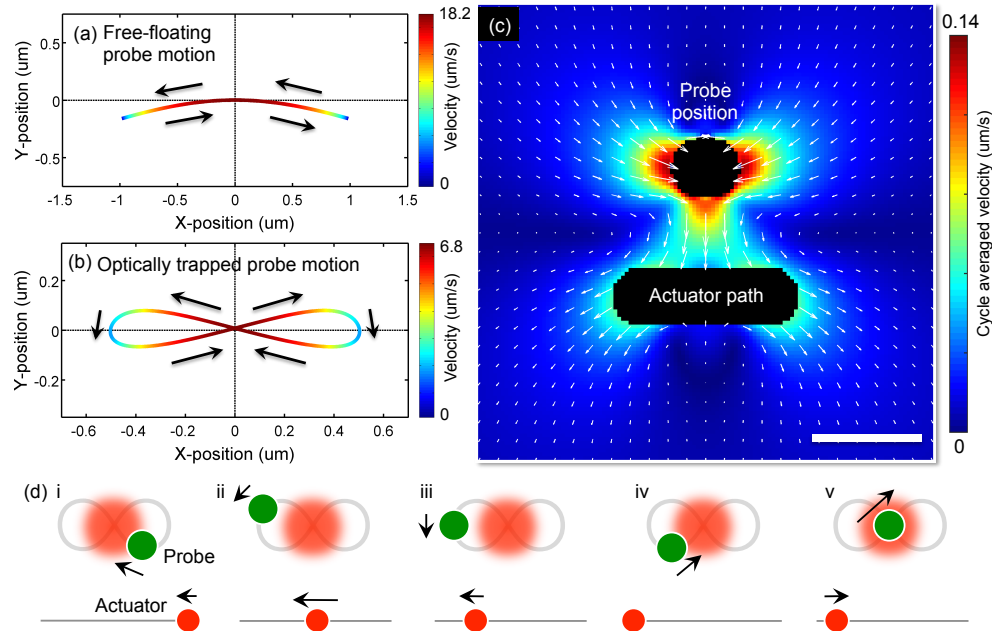


Fig. 3. Simulations of the system with a time-reversal symmetric actuator trajectory. (a) The time-reversal symmetric trajectory and velocity of the free-floating probe. (b) The motion of the probe with the introduction of a second stationary optical trap constraining its motion. Here time-reversal symmetry is broken as the probe follows a particular direction around the ‘figure of 8’ trajectory. (c) The cycle averaged flow-field of the system in a plane through the centre of both the actuator and probe microsphere. The white scale bar represents $10\text{ }\mu\text{m}$. (d) A schematic showing the relative positions of the actuator and probe microspheres through one actuator cycle. Once again the relative size of the probe trajectory has been exaggerated compared to both the probe size, and the actuator trajectory, for clarity.

Any non zero cycle-averaged flows can now be directly attributed to the presence of the stationary optical trap. Figure 3(b) shows the trajectory of the probe microsphere when constrained by a stationary optical trap. This ‘figure of 8’ trajectory is *not* time-reversible: the probe microsphere always proceeds around the path in a particular direction. As discussed in Section 1, the breaking of time-reversal symmetry is accompanied by the generation of a non-zero cycle averaged flow, which in this case corresponds to a small flow induced by the presence of the second optical trap, as shown in Fig. 3(c). Interestingly, the reflection symmetry of the system (along a vertical line through the centre of Fig. 3(c)) dictates that the cycle averaged flow is directed *orthogonally* to the direction of motion of the actuator.

We note that in all of the simulations presented here, the probe particle remains within the linear Hookean restoring force regime: for example the probe is $5\text{ }\mu\text{m}$ in diameter, but only moves a maximum distance of $\sim 0.8\text{ }\mu\text{m}$ away from the trap centre [14]. In the schematics shown in Fig. 1(a), Fig. 2(d) and Fig. 3(d), the scale of the probe’s trajectory has been exaggerated relative to the probe’s diameter for clarity. However in reality, the trajectory more resembles a ‘wobble’ than depicted in these schematics.

2.4. Energy transfer between the actuator and probe microspheres

The flow-field created by the breaking of time-reversal symmetry is due to the storage of energy in the probe bead (by pulling it away from its equilibrium position) which is then dissipated into the surrounding fluid later in the cycle. To investigate this further we now consider the energy transferred between the two microspheres in the system. Energy transfer between hydrodynamically coupled microspheres has previously been considered for the case of two particles held out of equilibrium at different effective temperatures [31]. In our case, the hydrodynamic flow generated by the actuator does work on the optically trapped probe microsphere to move it away from its equilibrium position in the harmonic potential of the stationary optical trap. The work done on the probe microsphere during each cycle, W , can be calculated from the line integral

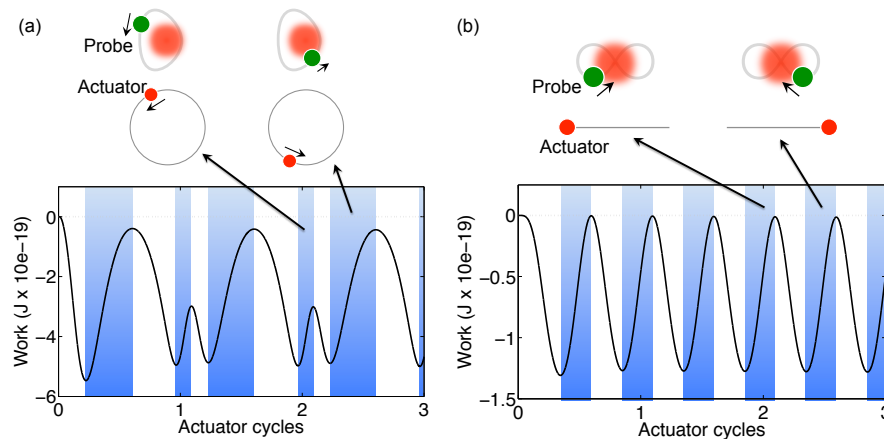


Fig. 4. Simulation of the work done on the probe microsphere in the absence of Brownian motion. (a) non time-reversal symmetric case. (b) time-reversal symmetric case. Each case shows the evolution of the energy stored in the system when the probe is initially positioned at rest at the centre of the trap. In (a), the probe orbits the centre of the trap, and at no point in its cycle does it revisit the trap centre, and consequently the curve never returns to zero as the stored energy is never fully released. The insets show the points in the trajectory where energy is released. Full schematics of the trajectories are shown in Fig. 2(d) and Fig. 3(d).

of the hydrodynamic vector field:

$$W = \oint_C \mathbf{F}_{hydro}(\mathbf{r}) \cdot d\mathbf{r} = \oint_C \mathbf{F}_{hydro}(\mathbf{r}(t)) \cdot \frac{d\mathbf{r}}{dt} dt, \quad (2)$$

where $\mathbf{F}_{hydro}(\mathbf{r}(t))$ is the time-dependent hydrodynamic vector flow-field (which varies throughout the cycle), $d\mathbf{r}(t)/dt$ describes the velocity of the probe when at position $\mathbf{r}(t)$ along its closed loop trajectory, and t is time. Equation (2) can be integrated numerically in our simulation, and the work done on the optically trapped probe microsphere under non time-reversal symmetric, and time-reversal symmetric driving configurations is shown in Fig. 4.

In our simulation we assume that the trap is conservative and so the energy dissipation is path independent [32]. The unshaded regions in Fig. 4(a) and 4(b) show the parts of the cycle where the probe is pushed away from the centre of the optical trap by the hydrodynamic flow, storing energy in the system (analogous to the storage of energy in an extended spring). The light blue shaded regions show the parts of the cycle where the probe moves closer to the centre of the optical trap, releasing the stored energy into the surrounding fluid. The repeated storage and release of energy per cycle is the mechanism by which the flow in the system is modified

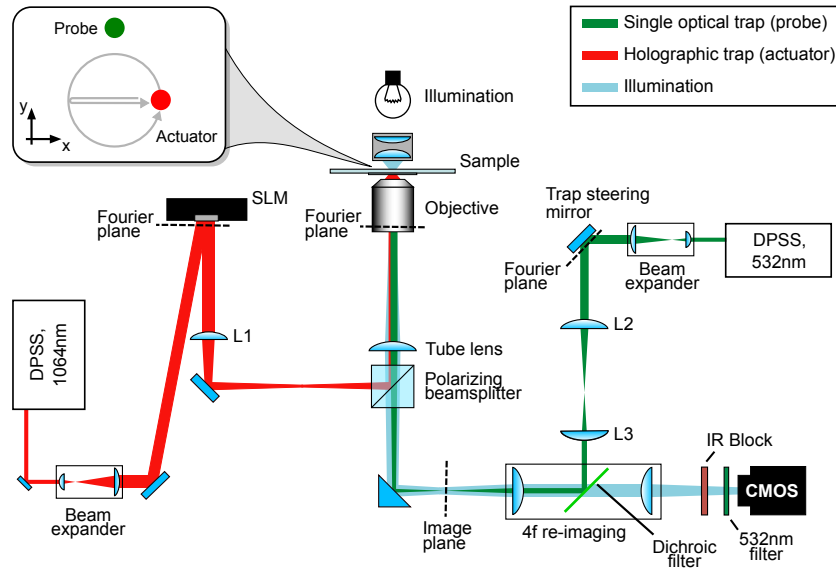


Fig. 5. Schematic of the dual beam holographic optical tweezers system. Our optical tweezers system is built around a custom-made inverted microscope with a Zeiss halogen illumination module (100 Watt). The holographic actuator trap is created by expanding a diode pumped solid state (DPSS) infra-red 1064 nm wavelength laser beam to overfill a nematic liquid crystal spatial light modulator (SLM) (BNS XY series, 512 x 512 pixels, 200Hz frame-rate). The SLM is placed in the Fourier plane of the sample and telescopically re-imaged onto and overfilling the back aperture of the objective lens (Nikon 100 x oil immersion, 1.3 NA) using a Fourier lens (L1) of 250 mm focal length and a tube lens of focal length 100 mm. The single beam trap is provided by a green DPSS 532 nm wavelength laser. Its position can be manually controlled using a steering mirror, and it also overfills the back aperture of the objective lens. The sample is viewed using a high-speed CMOS camera (Dalsa Genie gigabit ethernet), and any reflected infra-red and green laser light is filtered out. The top left inset shows a schematic of the relative optical trap positions and trajectories within the sample.

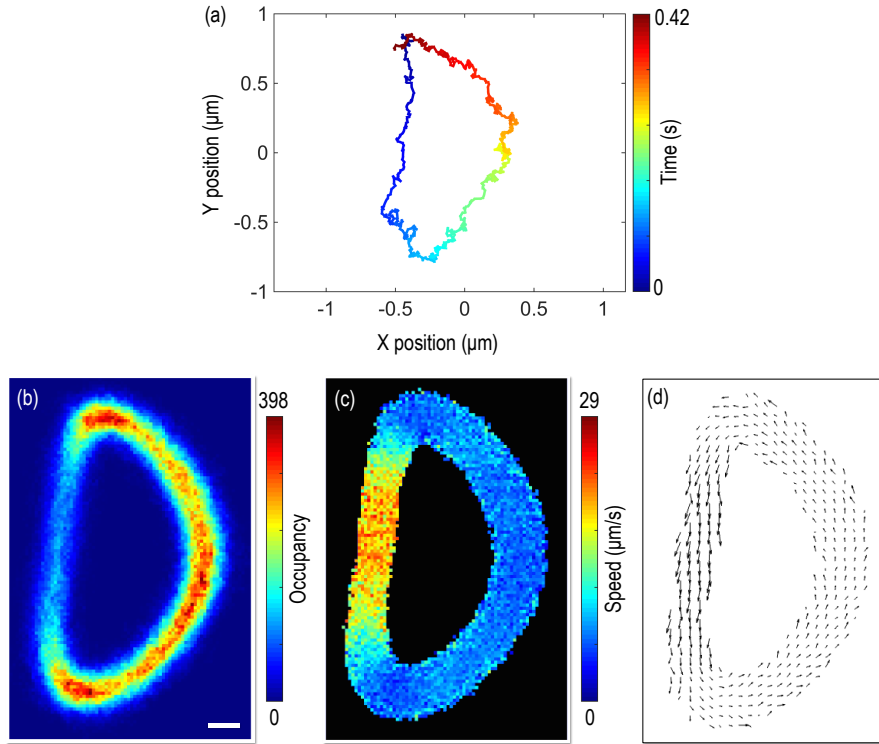


Fig. 6. Experimentally measured probe microsphere trajectories when subjected to a non-time-reversible flow-field. (a) The trajectory of the probe over a single non time-reversal symmetric actuator cycle. (b) A 2D occupancy histogram showing the number of visits the probe made to each 10 nm wide bin over the course of 100 actuator cycles. The white scale bar represents 100 nm. (c) The average drift velocity of the probe as it passes through each 10 nm x 10 nm histogram bin. (d) The magnitude and direction of the drift velocity of the probe bead.

when the second optical trap is introduced.

3. Experimental validation

We now describe experimental measurements that we performed to verify the findings of our simulations. The holographic optical tweezers system [33] used in this work is based upon that described in [34] and our modifications are described in the caption of Fig. 5. We used two independent lasers to create the holographically controlled actuator trap (red) and the single beam probe trap (green), in order to prevent any coupling between the beams. By updating the hologram pattern on the SLM, designed using the ‘gratings and lenses’ algorithm [35, 36], the holographic actuator trap can be driven around circular or sinusoidal trajectories as required. We trap two 5 μm diameter silica microspheres, and track the 2D centroid of the probe microsphere at 2.5 kHz by finding the centre of symmetry of high-speed video images. In these experiments the amplitude of the actuator trajectory was 7.5 μm , and the probe trap was positioned 15 μm from the centre of the actuator trajectory. The actuator cycle rate was 2.4 Hz. The 2D stiffness $\mathbf{k} = (k_x, k_y)$ of the probe trap was measured using the Equipartition method and found to be: $k_x = 3.1 \pm 0.24 \times 10^{-6} \text{ N/m}$, and $k_y = 2.8 \pm 0.35 \times 10^{-6} \text{ N/m}$. The experiments were conducted

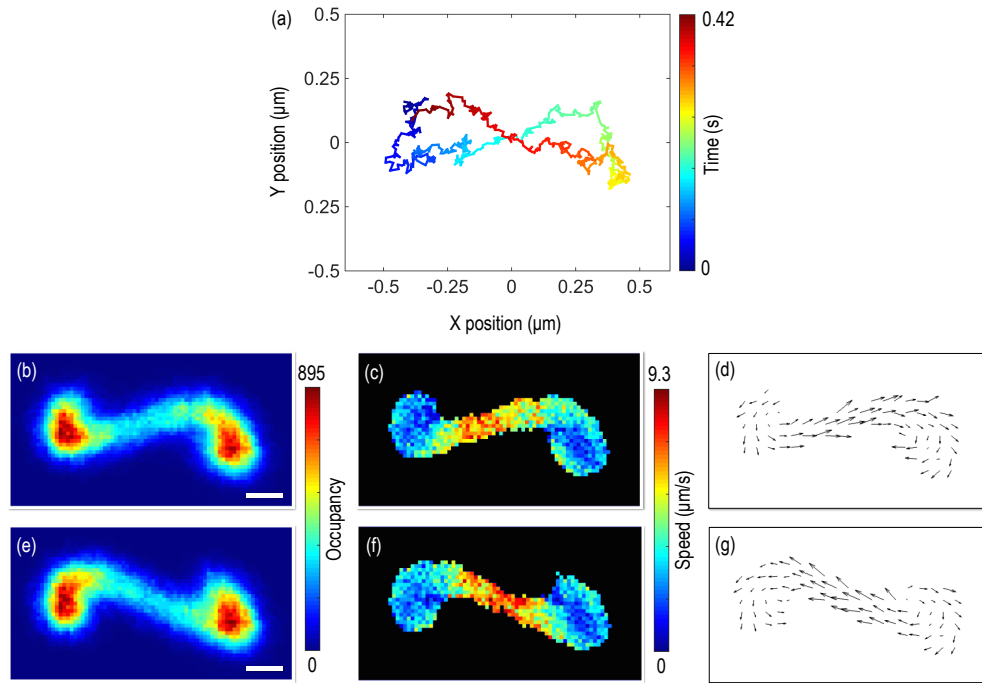


Fig. 7. Experimentally measured probe microsphere trajectories when subjected to a time-reversible flow-field. (a) The trajectory of the probe over a single time-reversal symmetric actuator cycle. (b) and (e) 2D occupancy histograms showing the number of visits the probe made to each 10 nm wide bin over the course of 100 actuator cycles. The white scale bars represent 100 nm. (b) is the first half of the cycle, (e) is the second half of the cycle. (c) and (f) The average drift velocity of the probe as it passes through each 10 nm x 10 nm histogram bin. (d) and (g) The magnitude and direction of the drift velocity of the probe bead.

$\sim 30 \mu\text{m}$ away from the bottom of the sample.

Figures 6 and 7 show the experimentally measured response of the optically trapped probe microsphere as it is subjected to the two types of flow-field generated by the actuator. In the experiments the microspheres also experience the stochastic forces of Brownian motion. In order to average out the effect of Brownian motion, we observe the probe over 100 actuator cycles, and construct an occupancy histogram displaying the number of visits the probe made to each of a 2D grid of 10 nm x 10 nm bins. These histograms are shown in Fig. 6(b) and Figs. 7(b) and 7(c). For the time-reversal symmetric actuator motion, the data is displayed in two plots to separate the probe's motion in the first and second half of each cycle, as it revisits the central region twice per cycle. The histogram occupancy maps are approximately inversely proportional to the probe's speed. We also calculate the average drift velocity of the probe as it passes through each histogram bin, which is shown in Figs. 6(c) and 6(d) and Figs. 7(c), 7(d), 7(f) and 7(g). Both the shape and the relative velocity of the probe's trajectories agree well with those predicted by simulation in Fig. 2(c) and Fig. 3(b). We stress that the measured 'figure of 8' trajectory followed by the probe particle in this experiment is a *signature* of the breaking of time-reversal symmetry in the system. This trajectory can *only* occur if a small non-time symmetric flow-field is *also* generated, which results in a weak pumping action of the system.

4. Conclusions

In this paper we have investigated ‘Lissajous-like’ trajectories of free-floating and optically trapped particles as they experience oscillating hydrodynamic forces. In particular, we have demonstrated the breaking of time-reversal symmetry in the motion of an optically trapped particle when it is subjected to a time-reversible external force-field. This symmetry breaking results in a fluid pumping action of the system, in a direction orthogonal to that of the original driving actuator motion. Unlike earlier studies investigating synchronisation [6, 9, 29], in this paper the actuator is *not* driven with a constant or prescribed force profile which requires feedback to realise position- or force-clamping. In our experiments, the stiffness of the actuator trap was approximately 1 order of magnitude larger than that of the probe trap. The stiffness of the actuator trap is not an important parameter in determining the behaviour of the system, as long as the actuator bead is trapped stiffly enough so that it can keep up with the oscillatory motion of the actuator trap. The trajectories followed by the probe microsphere are independent of the initial conditions (such as the initial phase of the actuator) after a few actuator cycles. The symmetry breaking is a consequence of the action of both a time-dependent external force (in this case hydrodynamic), and a position-dependent restoring force as the microsphere moves within the harmonic potential of the optical trap. Throughout its motion, the trapped particle never reaches a static equilibrium position. We have shown how energy is stored as the particle is pulled away from its equilibrium position, and then dissipated into the surrounding fluid later in the cycle when the particle moves back towards the centre of the trap. This effect is subtle: in the cases described here generating flow rates on the order of $0.1\mu\text{m/s}$, which is $\sim 0.2\%$ of the maximum actuator speed. The effect may play a role on the dynamic evolution of systems as optical tweezers measurements become ever more delicate, or in more complicated systems consisting of a greater number of interacting particles, such as multipoint velocity measurements. The results presented here also point towards methods to *hydrodynamically* manipulate free-floating objects using flows generated by nearby optically trapped particles [27].

Acknowledgments

This work was supported by the EPSRC (grant number EP/I007822/1). M.J.P. would like to thank the Royal Society and the Wolfson Foundation. We would also like to thank Dr Jonathan Taylor and Dr Michael Lee for useful discussions.